A numerical study of 2D integrated RBFNs incorporating Cartesian grids for solving 2D elliptic differential problems

N. Mai-Duy* and T. Tran-Cong

Computational Engineering and Science Research Centre

Faculty of Engineering and Surveying,

The University of Southern Queensland, Toowoomba, QLD 4350, Australia

Submitted to *Numerical Methods for Partial Differential Equations*,

15-Dec-2008; revised, 25-May-2009

Short title: 2D-IRBFN Cartesian-grid technique

*Corresponding author: Telephone +61 7 4631 1324, Fax +61 7 4631 2526, E-mail maiduy@usq.edu.au

Abstract This paper reports a numerical discretisation scheme, based on two-dimensional integrated radial-basis-function networks (2D-IRBFNs) and rectangular grids, for solving second-order elliptic partial differential equations defined on 2D non-rectangular domains. Unlike finite-difference and 1D-IRBFN Cartesian-grid techniques, the present discretisation method is based on an approximation scheme that allows the field variable and its derivatives to be evaluated anywhere within the domain and on the boundaries, regardless of the shape of the problem domain. We discuss the following two particular strengths, which the proposed Cartesian-grid-based procedure possesses, namely (i) the implementation of Neumann boundary conditions on irregular boundaries and (ii) the use of high-order integration schemes to evaluate flux integrals arising from a control-volume discretisation on irregular domains. A new preconditioning scheme is suggested to improve the 2D-IRBFN matrix condition number. Good accuracy and high-order convergence solutions are obtained.

Keywords: integrated radial basis function network; Cartesian grid; irregular domain; Neumann boundary condition; control-volume discretisation; point-collocation discretisation

1 INTRODUCTION

Discretisation techniques require the replacement of the domain of interest with a union of small elements, a collection of control volumes, a Cartesian grid or a set of discrete points. Generating a Cartesian grid or a set of discrete points is seen to be much more economical than generating a finite-element mesh, particularly for the case of irregularly-shaped domains. As a result, considerable effort has been put into the development of Cartesian-grid-based techniques and meshless techniques.

This study is concerned with the development of a Cartesian-grid-based technique. For

Cartesian-grid techniques, difficulties lie in the handling of irregular boundary geometries. Since the irregular boundary does not generally pass through grid nodes (regular points), one expects to have a change in grid spacing in all directions for interior points adjacent to the boundary. It has been shown that a rapid change of the grid size can result in a substantial deterioration in accuracy (e.g. [1]). A variety of techniques have been explored to overcome this problem. Examples include higher-order boundary fitting schemes, where error bounds for the quadratic boundary treatment are derived, (e.g. [2,3]) and embedded boundary techniques (e.g. [4,5]). There are further complications for the case of Neumann boundary conditions. Expressions for computing a gradient boundary condition embrace first-order derivatives in both coordinate directions. However, at an irregular boundary point, one is given explicitly information about the change of the field variable in one coordinate direction only. Special treatments are required. Typically, supplementary approximations are introduced at the boundary (e.g. [6-8]) or rectangular grids are formed in a way that boundary points are also grid nodes (e.g. [9]). If one uses a control-volume approach (subregion collocation) for the discretisation, the accuracy of the technique depends on both the approximation of gradients (e.g. diffusive fluxes) and the evaluation of integrals involving these gradients. For the latter, assume that the flux evaluations are sufficiently accurate, the midpoint rule is capable of yielding second-order accuracy only as discussed in [10].

Radial-basis-function networks (RBFNs) are known as a powerful tool for the approximation of scattered data. Their application to the solution of partial differential equations (PDEs) has received a great deal of attention over the last 15 years (e.g. [11] and references therein). It is easy to implement RBF collocation methods and they can give a high-order convergence solution. On the other hand, the RBF matrices are fully populated and their condition numbers grow quickly with increasing number of RBF centres. A number of approaches, such as local approximations (e.g. [12,13]), domain decompositions (e.g. [14-16]), preconditioning schemes (e.g. [17]) and compactly-supported RBFs (e.g. [18,19]), have been presented, towards the solution of large-scale problems.

Integrated RBFNs (IRBFNs) have some advantages over differentiated RBFNs (DRBFNs) in certain types of problems such as those involving the approximation of high-order derivatives, the implementation of multiple boundary conditions, and the enforcement of second-order continuity of the approximate solution across the subdomain interfaces (e.g. [20-22]). In the context of Cartesian-grid techniques, IRBFNs were employed to represent the field variable on each grid line (1D-IRBFNs), which allows a larger number of nodes to be employed (e.g. [23-25]). Because 1D-IRBFN approximation schemes with respect to the two coordinate directions are independent, difficulty is encountered for irregular domains when one tries to implement normal derivative boundary conditions and use Gaussian quadrature to evaluate flux integrals. In [24], a technique for generating a non-uniform grid where the boundary points coincide with regular mesh points [9] was adopted to implement Neumann boundary conditions. In this paper, we discuss the use of 2D-IRBFNs over the whole domain that has the ability to overcome these difficulties. Furthermore, a new preconditioning scheme and a hybrid numerical procedure are proposed to enhance the performance of the present Cartesian-grid-based technique.

The remainder of the paper is organised as follows. In Section 2, a brief review of integrated RBFNs is given. In Section 3, the proposed Cartesian-grid-based technique incorporating 2D-IRBFNs is described and its performance is investigated numerically. Emphasis is placed on the discussion about some strengths and weaknesses of 2D-IRBFNs in the context of Cartesian-grid-based techniques. Section 4 concludes the paper.

2 TWO-DIMENSIONAL INTEGRATED RBFNs ON CARTESIAN GRIDS

In the remainder of the paper, we will use

- the notation $\widehat{[]}$ for a vector/matrix $[]$ that is associated with 1D-IRBFNs, a grid line or a segment of the boundary,
- the notation $\widetilde{[]}$ for a vector/matrix $[]$ that is associated with 2D-IRBFNs or the whole set of grid lines,
- the notation $[]_{(\eta)}$ to denote selected rows η of the vector $[]$,
- the notation $[]_{(\eta,\theta)}$ to denote selected rows η and columns θ of the matrix $[]$,
- the notation $[]_{(:,\theta)}$ to denote all rows of the matrix $[]$,
- the notation $[]_{(\eta,:)}$ to denote all columns of the matrix $[]$, and
- the notation cond($[]$) to denote the the 2-norm condition number of the matrix $[]$.

The domain of interest, which can be rectangular or non-rectangular, is embedded in a Cartesian grid of density $N_1 \times N_2$. In the case of non-rectangular domains, grid nodes outside the domain are removed. Boundary points are generated through the intersection of the grid lines and the boundaries of the domain. The construction of the RBF approximations can be based on differentiation or integration. For the latter, which is employed in this study, the highest-order derivatives of the field variable in a given PDE are decomposed into RBFs. Approximate expressions for lower-order derivatives and the field variable itself are then obtained through integration. For the solution of second-order PDEs on 2D domains, the integral scheme will start with

$$\frac{\partial^2 u(\mathbf{x})}{\partial x_j^2} = \sum_{i=1}^{N} w^{(i)} G^{(i)}(\mathbf{x}), \qquad (1)$$

where u is the field variable, $\mathbf{x}$ the position vector, x_j the j-component of $\mathbf{x}$ ($j = [1, 2]$), N the number of RBF centres (interior and boundary points) associated with the x_j grid lines ($N = N_1 N_2$ for a rectangular domain), w the network weight and $G(\mathbf{x})$ the RBF.

Integrating (1) with respect to x_j leads to

$$\frac{\partial u(\mathbf{x})}{\partial x_j} = \sum_{i=1}^{N} w^{(i)} H^{(i)}(\mathbf{x}) + C_1(x_k), \tag{2}$$

$$u(\mathbf{x}) = \sum_{i=1}^{N} w^{(i)} \overline{H}^{(i)}(\mathbf{x}) + x_j C_1(x_k) + C_2(x_k), \tag{3}$$

where $H = \int G dx_j$, $\overline{H} = \int H dx_j$, and C_1 and C_2 are the constants of integration which are univariate functions of the variable other than x_j (i.e. x_k ($k \neq j$)). For points lying on a grid line that is parallel to the x_j direction, expressions (2) and (3) will have the same values of C_1 and C_2.

We also employ IRBFNs to represent the variation of the constants of integration. These approximate functions are expressed in terms of the nodal values of C_1 and C_2 (the physical space) rather than in terms of the RBF weights/coefficients used in past work (e.g. [26]).

The construction process for $C_1(x_k)$ is exactly the same as that for $C_2(x_k)$. To simplify the notation, some subscripts are dropped. The function $C(x_k)$ is constructed through

$$\frac{d^2 C(x_k)}{dx_k^2} = \sum_{i=1}^{N_k} w^{(i)} g^{(i)}(x_k), \tag{4}$$

$$\frac{dC(x_k)}{dx_k} = \sum_{i=1}^{N_k} w^{(i)} h^{(i)}(x_k) + c_1, \tag{5}$$

$$C(x_k) = \sum_{i=1}^{N_k} w^{(i)} \bar{h}^{(i)}(x_k) + x_k c_1 + c_2, \tag{6}$$

where c_1 and c_2 are the constants of integration which are simply unknown numbers, and $g^{(i)}$, $h^{(i)}$ and $\bar{h}^{(i)}$ the one-dimensional form of $G^{(i)}$, $H^{(i)}$ and $\overline{H}^{(i)}$, respectively.

Collocating (6) at the local grid points $x_k^{(i)}$ with $i = \{1, 2, \cdots, N_k\}$ leads to

$$\widehat{C} = \widehat{\mathcal{T}} \begin{pmatrix} \widehat{w} \\ c_1 \\ c_2 \end{pmatrix}, \tag{7}$$

where $\widehat{C}$ and $\widehat{w}$ are the vectors of length N_k, and $\widehat{\mathcal{T}}$ the transformation matrix of dimensions $N_k \times (N_k + 2)$

$$\widehat{C} = \left(C(x_k^{(1)}), C(x_k^{(2)}), \cdots, C(x_k^{(N_k)})\right)^T = \left(C^{(1)}, C^{(2)}, \cdots, C^{(N_k)}\right)^T,$$

$$\widehat{w} = \left(w^{(1)}, w^{(2)}, \cdots, w^{(N_k)}\right)^T,$$

$$\widehat{\mathcal{T}} = \begin{bmatrix} \bar{h}^{(1)}(x_k^{(1)}), & \bar{h}^{(2)}(x_k^{(1)}), & \cdots, & \bar{h}^{(N_k)}(x_k^{(1)}), & x_k^{(1)}, & 1 \\ \bar{h}^{(1)}(x_k^{(2)}), & \bar{h}^{(2)}(x_k^{(2)}), & \cdots, & \bar{h}^{(N_k)}(x_k^{(2)}), & x_k^{(2)}, & 1 \\ \vdots & \vdots & \ddots & \vdots & \vdots & \vdots \\ \bar{h}^{(1)}(x_k^{(N_k)}), & \bar{h}^{(2)}(x_k^{(N_k)}), & \cdots, & \bar{h}^{(N_k)}(x_k^{(N_k)}), & x_k^{(N_k)}, & 1 \end{bmatrix}.$$

Taking (7) into account, the value of (6) at an arbitrary point x_k can be computed in terms of nodal values of C as

$$C(x_k) = \left[\bar{h}^{(1)}(x_k), \bar{h}^{(2)}(x_k), \cdots, \bar{h}^{(N_k)}(x_k), x_k, 1\right] \widehat{\mathcal{T}}^+ \widehat{C}, \tag{8}$$

or

$$C(x_k) = \sum_{i=1}^{N_k} P^{(i)}(x_k) C^{(i)}, \tag{9}$$

where $P^{(i)}(x_k)$ is the product of the first vector on RHS of (8) and the ith column of $\widehat{\mathcal{T}}^+$, and $\widehat{\mathcal{T}}^+$ the generalised inverse of $\widehat{\mathcal{T}}$ of dimensions $(N_k + 2) \times N_k$. Approximate expressions $C_1(x_k)$ and $C_2(x_k)$ thus contain N_k terms only.

Substitution of (9) into (2) and (3) yields

$$\frac{\partial u(\mathbf{x})}{\partial x_j} = \sum_{i=1}^{N} w^{(i)} H^{(i)}(\mathbf{x}) + \sum_{i=1}^{N_k} P^{(i)}(x_k) C_1^{(i)}, \tag{10}$$

$$u(\mathbf{x}) = \sum_{i=1}^{N} w^{(i)} \overline{H}^{(i)}(\mathbf{x}) + \sum_{i=1}^{N_k} x_j P^{(i)}(x_k) C_1^{(i)} + \sum_{i=1}^{N_k} P^{(i)}(x_k) C_2^{(i)}. \tag{11}$$

For convenience of presentation, expressions (1), (10) and (11) can be rewritten as

$$\frac{\partial^2 u(\mathbf{x})}{\partial x_j^2} = \sum_{i=1}^{N+2N_k} w^{(i)} G^{(i)}(\mathbf{x}), \tag{12}$$

$$\frac{\partial u(\mathbf{x})}{\partial x_j} = \sum_{i=1}^{N+2N_k} w^{(i)} H^{(i)}(\mathbf{x}), \tag{13}$$

$$u(\mathbf{x}) = \sum_{i=1}^{N+2N_k} w^{(i)} \overline{H}^{(i)}(\mathbf{x}), \tag{14}$$

where

$$\{G^{(i)}(\mathbf{x})\}_{i=N+1}^{N+2N_k} \equiv \{0\}_{i=1}^{2N_k},$$

$$\{H^{(i)}(\mathbf{x})\}_{i=N+1}^{N+N_k} \equiv \{P^{(i)}(x_k)\}_{i=1}^{N_k},$$

$$\{H^{(i)}(\mathbf{x})\}_{i=N+N_k+1}^{N+2N_k} \equiv \{0\}_{i=1}^{N_k},$$

$$\{\overline{H}^{(i)}(\mathbf{x})\}_{i=N+1}^{N+N_k} \equiv \{x_j P^{(i)}(x_k)\}_{i=1}^{N_k},$$

$$\{\overline{H}^{(i)}(\mathbf{x})\}_{i=N+N_k+1}^{N+2N_k} \equiv \{P^{(i)}(x_k)\}_{i=1}^{N_k},$$

$$\{w^{(i)}\}_{i=N+1}^{N+N_k} \equiv \{C_1^{(i)}\}_{i=1}^{N_k}, \text{ and}$$

$$\{w^{(i)}\}_{i=N+N_k+1}^{N+2N_k} \equiv \{C_2^{(i)}\}_{i=1}^{N_k}.$$

We seek an approximate solution in terms of nodal values of the field variable. To do so, multiple spaces of the network weights will be transformed into the physical space.

Collocating (14) at the nodal points associated with the x_j grid lines, $\{\mathbf{x}^{(i)}\}_{i=1}^{N}$, leads to

$$\widetilde{\mathcal{T}}\begin{pmatrix}\widetilde{w}\\ \widehat{C}_1\\ \widehat{C}_2\end{pmatrix}=\widetilde{u}, \tag{15}$$

where $\widetilde{\mathcal{T}}$ is a $N\times(N+2N_k)$ matrix, $\widetilde{w}=\left(w^{(1)},w^{(2)},\cdots,w^{(N)}\right)^T$, $\widehat{C}_1=\left(C_1^{(1)},C_1^{(2)},\cdots,C_1^{(N_k)}\right)^T$, $\widehat{C}_2=\left(C_2^{(1)},C_2^{(2)},\cdots,C_2^{(N_k)}\right)^T$, and $\widetilde{u}=\left(u(\mathbf{x}^{(1)}),u(\mathbf{x}^{(2)}),\cdots,u(\mathbf{x}^{(N)})\right)^T$. The transformation matrix $\widetilde{\mathcal{T}}$ has the entries $\widetilde{\mathcal{T}}_{li}=\overline{H}^{(i)}(\mathbf{x}^{(l)})$ for $1\leq l\leq N$ and $1\leq i\leq(N+2N_k)$. It is noted that at a grid node $P^{(i)}(x_k^{(j)})$ is equal to 0 if $i\neq j$ and 1 if $i=j$.

Solving (15) for the coefficient vector yields

$$\begin{pmatrix}\widetilde{w}\\ \widehat{C}_1\\ \widehat{C}_2\end{pmatrix}=\widetilde{\mathcal{T}}^{+}\widetilde{u}, \tag{16}$$

where $\widetilde{\mathcal{T}}^{+}$ is the generalised inverse of $\widetilde{\mathcal{T}}$.

The values of first- and second-order derivatives of u at the nodal points associated with the x_j grid lines can then be computed in terms of nodal variable values as

$$\widetilde{\frac{\partial u}{\partial x_j}}=\widetilde{\mathcal{H}}\widetilde{\mathcal{T}}^{+}\widetilde{u}, \tag{17}$$

$$\widetilde{\frac{\partial^2 u}{\partial x_j^2}}=\widetilde{\mathcal{G}}\widetilde{\mathcal{T}}^{+}\widetilde{u}, \tag{18}$$

where $\widetilde{\mathcal{H}}$ and $\widetilde{\mathcal{G}}$ are $N\times(N+2N_k)$ matrices, derived from (13) and (12), respectively. Their corresponding entries are $\widetilde{\mathcal{H}}_{li}=H^{(i)}(\mathbf{x}^{(l)})$ and $\widetilde{\mathcal{G}}_{li}=G^{(i)}(\mathbf{x}^{(l)})$ for $1\leq l\leq N$ and $1\leq i\leq(N+2N_k)$.

Expressions (17) and (18) can be rewritten in compact form

$$\widetilde{\frac{\partial u}{\partial x_j}} = \widetilde{\mathcal{D}}'_j \widetilde{u}, \qquad (19)$$

$$\widetilde{\frac{\partial^2 u}{\partial x_j^2}} = \widetilde{\mathcal{D}}''_j \widetilde{u}, \qquad (20)$$

where $\widetilde{\mathcal{D}}'_j = \widetilde{\mathcal{H}}\widetilde{\mathcal{T}}^+$ and $\widetilde{\mathcal{D}}''_j = \widetilde{\mathcal{G}}\widetilde{\mathcal{T}}^+$ are the first and second-order differentiation matrices in the physical space.

Consider a Poisson equation $\nabla^2 u = b$ with Dirichlet boundary conditions. Using point collocation, it can be transformed into

$$\widetilde{\mathcal{A}}\widetilde{u}_{(\theta)} = \left(\widetilde{\mathcal{D}}''_{1(\eta,\theta)} + \widetilde{\mathcal{D}}''_{2(\eta,\theta)}\right)\widetilde{u}_{(\theta)} = \widetilde{b}_{(\eta)}, \qquad (21)$$

where $\widetilde{\mathcal{A}}$ is the system matrix, and η and θ the two sets of indices representing the interior points. It is noted that η and θ are identical and the nomenclature was given at the beginning of this section. The integral solution procedure involves computing the transformation matrix $\widetilde{\mathcal{T}}$ and the system matrix $\widetilde{\mathcal{A}}$. From a computational point of view, it is desirable to have $\widetilde{\mathcal{T}}$ and $\widetilde{\mathcal{A}}$ with low condition numbers.

3 PROPOSED CARTESIAN-GRID TECHNIQUE

The problem domain is simply discretised using a Cartesian grid (i.e. an array of the x_1 and x_2 grid lines), on which 2D-IRBFNs are constructed to represent the field variable. The governing equations are approximated by means of point collocation and subregion collocation. We study three particular issues here, namely the use of preconditioning schemes, the implementation of Neumann boundary conditions, and the evaluation of flux integrals. For all numerical examples presented in this study, the proposed technique is carried out with the multiquadric basis function whose form is

$$G^{(i)}(\mathbf{x}) = \sqrt{(\mathbf{x}-\mathbf{c}^{(i)})^T(\mathbf{x}-\mathbf{c}^{(i)}) + a^{(i)2}}, \tag{22}$$

where $\mathbf{c}^{(i)}$ and $a^{(i)}$ are the centre and width of the ith MQ basis function, respectively. The set of centres is chosen to be the same as the set of collocation points and the MQ width is taken to be the minimum distance between the ith centre and its neighbours. The error of the approximate solution u is measured through its discrete relative L_2 norm, denoted by $Ne(u)$. The convergence rate is calculated as $N_e(u) \approx \gamma h^{\alpha} = O(h^{\alpha})$ in which h is the grid size, and α and γ the exponential model's parameters.

3.1 An effective preconditioning scheme

Consider the transformation system (15). The numerical stability of this system is dependent on the condition number of $\widetilde{\mathcal{T}}$. In the case that $\widetilde{\mathcal{T}}$ is ill-conditioned, special treatments are required. In this study, we adopt a preconditioning approach. Both sides of (15) are multiplied by a matrix, denoted by $\widetilde{\mathcal{B}}$, that is close to the inverse of $\widetilde{\mathcal{T}}$.

We propose the use of one-dimensional IRBFNs (1D-IRBFNs) to construct the preconditioner $\widetilde{\mathcal{B}}$. For 1D-IRBFNs, the approximations are constructed "locally" on each grid line. On a grid line that is parallel to the x_j axis, the field variable u is sought in the form

$$u(x_j) = \sum_{i=1}^{M} w^{(i)}\overline{h}^{(i)}(x_j) + x_j c_1 + c_2, \tag{23}$$

where M is the number of RBF centres (interior and boundary points) on the grid line ($M = N_j$ for a rectangular domain), and $\overline{h}$, c_1 and c_2 defined as before. It can be seen that the number of RBFs used in (23) is much less than that in (3) (i.e. $M \ll N$). One can describe the transformation system for the 1D case as

$$\widehat{\mathcal{T}}\begin{pmatrix}\widehat{w}\\ c_1\\ c_2\end{pmatrix}=\widehat{u}, \tag{24}$$

or

$$\begin{pmatrix}\widehat{w}\\ c_1\\ c_2\end{pmatrix}=\widehat{\mathcal{T}}^{+}\widehat{u}, \tag{25}$$

where $\widehat{\mathcal{T}}^{+}$ is the generalised inverse of dimensions $(M+2)\times M$, and $\widehat{w}$ and $\widehat{u}$ the vectors of length M. The first M rows of $\widehat{\mathcal{T}}^{+}$ are associated with the values of w at the grid points and we use this sub-matrix to construct the preconditioner $\widetilde{\mathcal{B}}$. In the case of rectangular domains, the assembly process can be simply carried out by means of Kronecker tensor products. Assume that the grid node is numbered from bottom to top and from left to right. The preconditioner will take the form

$$\widetilde{\mathcal{B}}=\widehat{\mathcal{T}}(1:N_j,:)\otimes\mathbf{1}, \tag{26}$$

for $x_j\equiv x_1$, and

$$\widetilde{\mathcal{B}}=\mathbf{1}\otimes\widehat{\mathcal{T}}(1:N_j,:), \tag{27}$$

for $x_j\equiv x_2$. In (26) and (27), $\mathbf{1}$ represents a unit matrix of dimensions $N_2\times N_2$ and $N_1\times N_1$, respectively. For the case of non-rectangular domains, the assembly process is similar to that used in the finite-element method.

The transformation system (15) can be preconditioned as

$$\widetilde{\mathcal{B}}\widetilde{\mathcal{T}}\begin{pmatrix}\widetilde{w}\\ \widehat{C}_1\\ \widehat{C}_2\end{pmatrix}=\widetilde{\mathcal{B}}\widetilde{u}. \tag{28}$$

It leads to

$$\begin{pmatrix} \widetilde{w} \\ \widehat{C}_1 \\ \widehat{C}_2 \end{pmatrix} = \left(\widetilde{\mathcal{B}}\widetilde{\mathcal{T}}\right)^+ \widetilde{\mathcal{B}}\widetilde{u}. \tag{29}$$

The proposed preconditioning scheme is examined numerically for both rectangular and non-rectangular domains.

3.1.1 Rectangular domain

Consider a square domain $[0,1]^2$. The problem domain is replaced with a Cartesian grid as shown in Figure 1a. Condition numbers of the transformation matrix are computed for uniform grids, $[3 \times 3,\ 5 \times 5,\ \cdots,\ 95 \times 95]$. It can be seen from Figure 2 that the preconditioned transformation system has much lower condition numbers than the original system. At $N = 9025$, the proposed preconditioning scheme produces the condition number lower by about 4 orders of magnitude. The growth in the condition number is reduced from $O(N^{2.71})$ (unpreconditioning) to $O(N^{1.74})$ (preconditioning).

To study the numerical stability of the system matrix $\widetilde{\mathcal{A}}$, we consider the following Poisson equation

$$\frac{\partial^2 u}{\partial x_1^2}+\frac{\partial^2 u}{\partial x_2^2} = 4(1-\pi^2)\left[\sin(\pi(2x_1-1))\sinh(2x_2-1)+4\cosh(2(2x_1-1))\cos(2\pi(2x_2-1))\right], \tag{30}$$

subject to Dirichlet boundary conditions. The exact solution for this test problem is taken as

$$u_e = \sin(\pi(2x_1-1))\sinh(2x_2-1)+\cosh(2(2x_1-1))\cos(2\pi(2x_2-1)). \tag{31}$$

Figure 3 shows the variation of (31). To provide a basis for the assessment of the present technique, we also employ conventional RBFN techniques. Conventional techniques seek the solution in the RBF space so that their solution procedures involve computing the system matrix only. The field variable u is decomposed into RBFs, which are then differentiated to obtain expressions for its derivatives (differentiated RBFNs (DRBFNs)). We employ a set of RBFs for DRBFNs which is exactly the same as that for IRBFNs (i.e. both approaches have the same number of RBFs, centres and widths (grid spacing)). Grid employed are $[7\times 7, 11\times 11, \cdots, 71\times 71]$. Figure 4 shows that the IRBFN technique outperforms the DRBFN technique regarding both the matrix condition number and the accuracy. It is apparent that the present system matrix is much better conditioned. The condition number grows at the rate of $O(N^{1.10})$ and $O(N^{1.62})$ for IRBFNs and DRBFNs, respectively. At $N = 5041$, the gap is about 4 orders of magnitude between the two RBF techniques (i.e. 4.89×10^3 for IRBFNs and 2.58×10^7 for DRBFNs). In terms of accuracy, the integral and differential RBF techniques yield a convergence rate of $O(h^{3.73})$ and $O(h^{1.43})$ (h-the grid size), respectively.

Since IRBFNs do not require an underlying grid, the present method can also work with a non-uniform Cartesian grid. Such a discretisation is shown in Figure 1b. We employ several non-uniform grids, namely $[13 \times 13, 15 \times 15, \cdots, 59 \times 59]$. The IRBFN solution converges apparently as $O(h^{3.49})$, where h is the grid size of the interior region (Figure 5). Given a number of nodes (e.g. $N = 3481$), the case of using a non-uniform grid is more accurate than that of a uniform grid (e.g. 6.48×10^{-6} versus 5.01×10^{-5} for $Ne(u)$).

3.1.2 Non-rectangular domain

The domain of interest is a circular domain of radius 1/2. The governing equation and the exact solution are respectively taken as

$$\frac{\partial^2 u}{\partial x_1^2} + \frac{\partial^2 u}{\partial x_2^2} = 4(1-\pi^2)\left[\sin(2\pi x_1)\sinh(2x_2) + 4\cosh(4x_1)\cos(4\pi x_2)\right], \qquad (32)$$

$$u_e = \sin(2\pi x_1)\sinh(2x_2) + \cosh(4x_1)\cos(4\pi x_2). \qquad (33)$$

This problem has the same exact solution as the previous one, except that the centre of the domain is shifted from (1/2,1/2) to (0,0). The problem domain is embedded in a uniform Cartesian grid and the exterior grid nodes are removed (Figure 6). We generate boundary nodes through the intersection of the grid lines and the boundary. It can be seen that there may be some interior grid nodes that are very close to the boundary. We introduce a parameter Δ to study their effect on the solution accuracy. Interior nodes, which fall within a small distance Δ to the boundary, will be set aside. Values of Δ are chosen here as $h/4, h/6$ and $h/8$, where h is the grid size. In Figure 7, we show a plot of the condition number of the transformation matrix versus the number of grid points. It can be seen that the preconditioned system has a much lower condition number. Its rate is reduced from $O(N^{2.52})$ (unpreconditioning) to $O(N^{1.86})$ (preconditioning). Table 1 shows the condition number of the system matrix and the solution accuracy for different values of Δ. Calculations are carried out for uniform grids, $[7 \times 7, 13 \times 13, \cdots, 61 \times 61]$. It is apparent that Δ only has a little effect on $Ne(u)$ and cond$(\widetilde{\mathcal{A}})$. At $\Delta = h/8$, the present technique yields a fast rate of convergence of $O(h^{4.14})$ with the matrix condition number being in the range of 4.72×10^1 to 4.38×10^3.

3.2 Implementation of Neumann boundary conditions on non-rectangular boundaries

In the context of Cartesian-grid techniques, Neumann boundary conditions are known to be more difficult to handle than Dirichlet boundary conditions. It is particularly acute for the case of non-rectangular boundaries. It should be pointed out that the present approximations are constructed globally through basis functions that are defined in both x_1 and x_2 directions and they do not require an underlying mesh. As a result, the field variable and its derivatives can be evaluated at any point within the domain and on its boundaries, irrespective of the shape of the problem domain. This feature facilitates the straightforward implementation of Neumann boundary conditions on irregular boundaries.

We consider a domain with a curved boundary that is prescribed with gradient boundary condition (Figure 8). This curve is an arc, centered at the origin, from 0 to 90^0 with a radius of 1/2. The top and right sides of the domain have a unit length. The governing equation and the exact solution are taken to be the same as those used in the first example (i.e. (30) and (31)).

As mentioned earlier, boundary points are generated by the intersection of the grid lines and the boundaries. At boundary points created via the x_j grid lines, the values of $\partial^2 u/\partial x_j^2$ and $\partial u/\partial x_j$ are directly obtained from the networks associated with x_j (they are nodal values), while the values of $\partial^2 u/\partial x_k^2$ and $\partial u/\partial x_k$ $(k \neq j)$ are computed from the networks associated with x_k through interpolation.

A distinguishing feature of IRBFNs is that a set of their coefficients is larger owing to the presence of integration constants. The Neumann boundary conditions can be imposed in the final system or in the transformation system. A detailed implementation of the two approaches for 1D-IRBFNs was presented in [24]. The latter is adopted here and its implementation is similar to that for 1D-IRBFNs. In contrast to 1D-IRBFNs, 2D-IRBFNs do not require the boundary points be grid nodes. Consider the x_j network and let N_{bj} be the number of boundary points that are specified with gradient boundary condition. Collocating the governing equation at the grid points and $\partial u/\partial x_j$ at the boundary points of Neumann boundary condition, one has

$$\widetilde{\mathcal{T}} \begin{pmatrix} \widetilde{w} \\ \widehat{C}_1 \\ \widehat{C}_2 \end{pmatrix} = \begin{pmatrix} \widetilde{u} \\ \widehat{\frac{\partial u}{\partial x_j}} \end{pmatrix} = \begin{pmatrix} \widetilde{u} \\ \frac{1}{n_j}\left(\widehat{\frac{\partial u}{\partial n}} - n_k \widehat{\frac{\partial u}{\partial x_k}}\right) \end{pmatrix}, \tag{34}$$

where n_j and n_k are the two components of the outward normal unit vector $\mathbf{n}$ at a boundary point, $\widetilde{w}$, $\widehat{C}_1$, $\widehat{C}_2$ and $\widetilde{u}$ defined as before, $\widetilde{\mathcal{T}}$ the transformation matrix of dimensions $(N+N_{bj})\times(N+2N_k)$ with $\widetilde{\mathcal{T}}_{li} = \overline{H}^{(i)}(\mathbf{x}^{(l)})$ for $1 \leq l \leq N$ and $1 \leq i \leq (N+2N_k)$ and $\widetilde{\mathcal{T}}_{li} = H^{(i)}(\mathbf{x}_b^{(l)})$ for $(N+1) \leq l \leq (N+N_{bj})$ and $1 \leq i \leq (N+2N_k)$. In (34), derivative boundary conditions are forced to be satisfied exactly. The 2D-IRBFN system thus contains information about Neumann boundary condition.

Condition numbers and errors are listed in Table 2. It can be seen that the present technique yields a fast rate of convergence. However, solutions to Neumann boundary-value problems are less stable than those to Dirichlet ones.

3.3 Implementation of high-order control-volume discretisations for non-rectangular domains

Consider a second-order PDE that involves the diffusive term only

$$\frac{\partial^2 u}{\partial x_1^2} + \frac{\partial^2 u}{\partial x_2^2} = 0, \tag{35}$$

on a circular domain of radius 1/2 centered at the origin, subject to Dirichlet boundary conditions. The exact solution is taken as

$$u_e(x_1, x_2) = \frac{1}{\sinh(\pi)} \sin\left(\pi x_1 + \frac{\pi}{2}\right) \sinh\left(\pi x_2 + \frac{\pi}{2}\right), \tag{36}$$

whose variation on $[-1/2, 1/2]^2$ is shown in Figure 9. The problem domain is represented by a Cartesian grid and each interior grid node is associated with a control volume defined by the x_1 and x_2 lines through the middle points of the grid node and its neighbours (Figure 10). For grid nodes adjacent to the boundary, relevant boundary points are used as their neigbours.

Integrating (35) over the ith control volume and applying the divergence theorem lead to

$$\int_{\Gamma_i} \left(\frac{\partial u}{\partial x} dy - \frac{\partial u}{\partial y} dx \right) = 0, \tag{37}$$

where Γ_i is the boundary of the control volume i. The field variable is represented by 2D-IRBFNs. The system of algebraic equations is generated by applying (37) to every interior grid node. We will study what effect the evaluation of integrals in (37) has on the solution accuracy. Two schemes, namely the midpoint rule and Gaussian quadrature with 5 points, are employed. To provide a basis for comparison, a control-volume approach described in [27] is also implemented. This approach, where the gradients are represented by linear functions and the boundary integrals are evaluated using the midpoint rule, is referred here as linear CVM.

Figure 11 and Table 3 show results obtained by linear-CVM (middle-point rule), IRBFN-CVMa (middle-point rule) and IRBFN-CVMb (5-point Gaussian quadrature). It is known that the middle-point rule is only an $O(h^2)$ method. One thus expects that IRBFN-CVMa is second-order accurate. As shown in Figure 11, although more accurate, the rate of IRBFN-CVMa is similar to that of linear-CVM. On the other hand, 5-point Gaussian quadrature is $O(h^{10})$ and the IRBFN-CVMb, as expected, outperforms linear-CVM and IRBFN-CVMa. In terms of cond($\widetilde{\mathcal{A}}$), IRBFN-CVMa has a slightly-larger condition number than linear-CVM and IRBFN-CVMb. The linear-CVM, IRBFN-CVMa and IRBFN-CVMb have respectively their observed rates as $O(N^{1.05})$, $O(N^{1.09})$ and $O(N^{1.06})$ for the condition number and $O(h^{1.96})$, $O(h^{2.10})$ and $O(h^{3.73})$ for the solution accuracy.

Comparing Table 3 with Table 1, it can be seen that the present control-volume approach is less sensitive to the parameter Δ than the present collocation approach. For all values of Δ, the present CV technique produces similar levels of accuracy.

3.4 Discussion

2D-IRBFNs have some strengths: (i) they allow the use of high-order integration schemes in the CV approach irrespective of the shape of the problem domain, and (ii) they have the ability to implement Neumann boundary conditions on irregular boundaries in a direct manner. However, the cost to construct 2D-IRBFNs is expensive. To alleviate this drawback, one can incorporate 1D-IRBFNs into the present Cartesian-grid numerical scheme. For rectangular regions, 1D-IRBFNs also permit the field variable and its derivatives to be evaluated at any point in the domain, and therefore one can use Gaussian quadrature for the control-volume formulation. The domain of complicated shape can thus be partitioned into a number of subdomains through a set of lines that are parallel to the x_1 and x_2 axes; one can then employ 2D- and 1D-IRBFNs to represent the solution in irregular and regular subdomains, respectively.

This domain decomposition procedure, which selectively exploits strengths of 1D- and 2D-IRBFNs, is numerically studied here through the domain shown in Figure 12. The geometry of Subdomain 1 is exactly the same as that used in Section 3.2, while Subdomain 2 is a unit square. Consider a Poisson equation with Dirichlet boundary conditions. The exact solution is created by making a simple coordinate transformation for (31) from $[0,1]^2$ to $[0,2] \times [0,1]$. We employ a control-volume approach with 5 Gaussian points to discretise the governing equation on each subdomain. The two subdomains are replaced with uniform rectangular grids of the same density. Subdomains 1 and 2 are handled with 2D- and 1D-IRBFNs, respectively. On the interface, the values of u at the interior points are taken as unknowns and they are found using continuity of the first-order normal derivative of the solution across the interface (the substructuring technique). Figure 13 presents two plots: (i) the condition number of the interface matrix, $\text{cond}(\widehat{\mathcal{A}}_f)$, versus the number of nodal points on the interface, N_f, and (ii) the solution accuracy, $Ne(u)$, for Subdomain 1, Subdomain 2 and the whole domain against the grid size, h. The interface matrix has relatively-low condition numbers, growing only at a rate of $O(N_f^{0.92})$. All errors are consistently reduced with decreasing grid size; these solutions converge apparently as $O(h^{3.70})$.

4 CONCLUDING REMARKS

This paper is concerned with the use of 2D-IRBFNs in the context of Cartesian-grid-based discretisation schemes for irregular domains. Some strengths and weaknesses of 2D-IRBFNs are discussed. 2D-IRBFNs have advantages in dealing with issues which require information on the field variable and its derivatives at points that do not coincide with regular grid nodes. Examples include the implementation of a Neumann boundary condition on irregular boundary and the use of high-order integration schemes in the control-volume framework. However, 2D-IRBFNs have higher matrix condition number and require more computational effort to construct than 1D-IRBFNs. For the former, an effective preconditioning scheme is developed. For the latter, a hybrid scheme is proposed, where 1D-IRBFNs are incorporated into the present Cartesian-grid procedure resulting in a much better computational efficiency. Numerical results indicate that there is a significant improvement in matrix condition number over convention RBFN methods, and very accurate results are achieved using relatively-coarse grids.

Acknowledgement

This work is supported by the Australian Research Council. We would like to thank the referees for their helpful comments.

References

1. F. G. Blottner, and P. J. Roache, Nonuniform mesh systems, Journal of Computational Physics 8 (1971), 498–499.

2. G. H. Shortley, and R. Weller, The numerical solution of Laplace's equation, Journal of Applied Physics 9 (1938), 334–344.

3. Z. Jomaa, and C. Macaskill, The embedded finite difference method for the Poisson equation in a domain with an irregular boundary and Dirichlet boundary conditions, Journal of Computational Physics 202(2) (2005), 488–506.

4. H. Johansen, and P. Colella, A Cartesian grid embedded boundary method for Poisson's equation on irregular domains, Journal of Computational Physics 147(1) (1998), 60–85.

5. P. Schwartz, M. Barad , P. Colella, and T. Ligocki, A Cartesian grid embedded boundary method for the heat equation and Poisson's equation in three dimensions, Journal of Computational Physics 211(2) (2006), 531–550.

6. R. V. Viswanathan, Solution of Poisson's equation by relaxation method–normal gradient specified on curved boundaries, Mathematical Tables and Other Aids to Computation 11(58) (1957), 67–78.

7. V. Thuraisamy, Approximate solutions for mixed boundary value problems by finite-difference methods, Mathematics of Computation 23(106) (1969), 373–386.

8. V. Thuraisamy, Monotone type discrete analogue for the mixed boundary value problem, Mathematics of Computation 23(106) (1969), 387–394.

9. E. Sanmiguel-Rojas, J. Ortega-Casanova, C. del Pino, and R. Fernandez-Feria, A Cartesian grid finite-difference method for 2D incompressible viscous flows in irregular geometries, Journal of Computational Physics 204(1) (2005), 302–318.

10. T. J. Moroney, and I. W. Turner, A finite volume method based on radial basis functions for two-dimensional nonlinear diffusion equations, Applied Mathematical Modelling 30(10) (2006), 1118–1133.

11. G. E. Fasshauer, Meshfree Approximation Methods With Matlab (Interdisciplinary Mathematical Sciences - Vol. 6), World Scientific Publishers, Singapore, 2007.

12. B. Sarler, and R. Vertnik, Meshfree explicit local radial basis function collocation method for diffusion problems, Computers & Mathematics with Applications 51(8) (2006), 1269–1282.

13. Y. V. S. S. Sanyasiraju, and G. Chandhini, Local radial basis function based gridfree scheme for unsteady incompressible viscous flows, Journal of Computational Physics 227(20) 2008, 8922-8948.

14. M. S. Ingber, C. S. Chen, and J. A. Tanski, A mesh free approach using radial basis functions and parallel domain decomposition for solving three-dimensional diffusion equations, International Journal for Numerical Methods in Engineering 60(13) (2004), 2183–2201.

15. J. Li, and Y.C. Hon, Domain decomposition for radial basis meshless methods, Numerical Methods for Partial Differential Equations 20 (2004), 450–462.

16. E. Divo, and A. Kassab, Iterative domain decomposition meshless method modeling of incompressible viscous flows and conjugate heat transfer, Engineering Analysis with Boundary Elements 30(6) (2006), 465–478.

17. L. Ling, and E. J. Kansa, Preconditioning for radial basis functions with domain decomposition methods, Mathematical and Computer Modelling 40(13) 2004, 1413–1427.

18. H. Wendland, Error estimates for interpolation by compactly supported radial basis functions of minimal degree, Journal of Approximation Theory 93(2) (1998), 258–272.

19. C. S. Chen, M. Ganesh, M. A. Golberg, and A. H. -D. Cheng, Multilevel compact radial functions based computational schemes for some elliptic problems, Computers

& Mathematics with Applications 43(3-5) (2002), 359–378.

20. N. Mai-Duy, Solving high order ordinary differential equations with radial basis function networks, International Journal for Numerical Methods in Engineering 62 (2005), 824–852.

21. N. Mai-Duy, and T. Tran-Cong, Solving biharmonic problems with scattered-point discretisation using indirect radial-basis-function networks, Engineering Analysis with Boundary Elements 30(2) (2006), 77–87.

22. N. Mai-Duy, and T. Tran-Cong, A multidomain integrated-radial-basis-function collocation method for elliptic problems, Numerical Methods for Partial Differential Equations 24(5) (2008), 1301–1320.

23. N. Mai-Duy, and R. I. Tanner, A collocation method based on one-dimensional RBF interpolation scheme for solving PDEs, International Journal of Numerical Methods for Heat & Fluid Flow 17 (2007), 165–186.

24. N. Mai-Duy, and T. Tran-Cong, A Cartesian-grid collocation method based on radial-basis-function networks for solving PDEs in irregular domains, Numerical Methods for Partial Differential Equations 23 (2007), 1192–1210.

25. N. Mai-Duy, and T. Tran-Cong, A control volume technique based on integrated RBFNs for the convection-diffusion equation, Numerical Methods for Partial Differential Equations (accepted).

26. N. Mai-Duy, and T. Tran-Cong, An efficient indirect RBFN-based method for numerical solution of PDEs, Numerical Methods for Partial Differential Equations 21 (2005), 770–790.

27. S. V. Patankar, Numerical Heat Transfer and Fluid Flow, McGraw-Hill, New York, 1980.

Table 1: Non-rectangular, point-collocation approach: Conditioner numbers of the system matrix and errors of the solution u. It is noted that $a(b)$ denotes $a \times 10^b$.

Grid	$\Delta = h/4$		$\Delta = h/6$		$\Delta = h/8$	
	cond($\widetilde{\mathcal{A}}$)	$Ne(u)$	cond($\widetilde{\mathcal{A}}$)	$Ne(u)$	cond($\widetilde{\mathcal{A}}$)	$Ne(u)$
7×7	2.08(+1)	1.94(-1)	4.72(+1)	1.18(-1)	4.72(+1)	1.18(-1)
13×13	1.12(+2)	3.18(-3)	1.76(+2)	5.15(-3)	1.76(+2)	5.15(-3)
19×19	2.65(+2)	8.39(-4)	2.65(+2)	8.39(-4)	2.65(+2)	8.39(-4)
25×25	4.81(+2)	2.21(-4)	4.81(+2)	2.21(-4)	4.81(+2)	2.21(-4)
31×31	7.58(+2)	1.48(-4)	7.74(+2)	1.25(-4)	1.43(+3)	9.74(-5)
37×37	1.09(+3)	5.23(-5)	1.35(+3)	6.32(-5)	1.35(+3)	6.32(-5)
43×43	1.49(+3)	3.24(-5)	1.86(+3)	3.67(-5)	1.86(+3)	3.67(-5)
49×49	1.95(+3)	2.81(-5)	1.95(+3)	1.52(-5)	3.13(+3)	1.54(-5)
55×55	2.48(+3)	1.41(-5)	3.40(+3)	1.29(-5)	4.51(+3)	1.13(-5)
61×61	3.06(+3)	7.69(-6)	4.38(+3)	7.70(-6)	4.38(+3)	7.70(-6)
	$O(N^{1.09})$	$O(h^{4.12})$	$O(N^{1.02})$	$O(h^{4.11})$	$O(N^{1.07})$	$O(h^{4.14})$

Table 2: Non-rectangular, point-collocation approach, Neumann boundary condition: Conditioner numbers of the system matrix and errors of the solution u. It is noted that $a(b)$ denotes $a \times 10^b$.

Grid	$\Delta = h/4$		$\Delta = h/6$		$\Delta = h/8$	
	cond$(\widetilde{\mathcal{A}})$	$Ne(u)$	cond$(\widetilde{\mathcal{A}})$	$Ne(u)$	cond$(\widetilde{\mathcal{A}})$	$Ne(u)$
7×7	2.27(+3)	2.34(+0)	2.27(+3)	2.34(+0)	2.77(+4)	1.72(+0)
13×13	5.97(+3)	2.86(-2)	5.97(+3)	2.86(-2)	5.97(+3)	2.86(-2)
19×19	3.80(+4)	2.32(-2)	6.22(+4)	1.24(-2)	6.22(+4)	1.24(-2)
25×25	1.43(+5)	6.62(-3)	2.74(+5)	1.21(-2)	2.71(+5)	1.22(-2)
31×31	2.29(+5)	4.17(-3)	1.12(+5)	3.47(-3)	1.08(+5)	3.00(-3)
37×37	3.84(+5)	3.62(-3)	3.83(+5)	3.69(-3)	3.83(+5)	3.69(-3)
43×43	4.15(+5)	1.70(-3)	7.39(+5)	9.53(-4)	7.39(+5)	9.53(-4)
49×49	3.09(+5)	6.00(-4)	3.22(+5)	3.70(-4)	7.27(+5)	7.08(-4)
55×55	1.32(+6)	3.37(-4)	1.81(+6)	6.85(-4)	1.80(+6)	6.84(-4)
61×61	7.86(+5)	3.26(-4)	9.42(+5)	3.64(-4)	1.10(+6)	3.65(-4)
	$O(N^{1.49})$	$O(h^{3.55})$	$O(N^{1.52})$	$O(h^{3.50})$	$O(N^{1.19})$	$O(h^{3.33})$

Table 3: Non-rectangular, control-volume approach, IRBFN-CVMb: Conditioner numbers of the system matrix and errors of the solution u. It is noted that $a(b)$ denotes $a \times 10^b$.

Grid	$\Delta = h/4$		$\Delta = h/6$		$\Delta = h/8$	
	cond($\widetilde{\mathcal{A}}$)	$Ne(u)$	cond($\widetilde{\mathcal{A}}$)	$Ne(u)$	cond($\widetilde{\mathcal{A}}$)	$Ne(u)$
7×7	1.16(+1)	2.85(-3)	1.13(+1)	2.61(-3)	1.13(+1)	2.61(-3)
13×13	5.10(+1)	2.17(-4)	4.85(+1)	2.08(-4)	4.85(+1)	2.08(-4)
19×19	1.10(+2)	4.70(-5)	1.10(+2)	4.70(-5)	1.10(+2)	4.70(-5)
25×25	1.97(+2)	1.57(-5)	1.97(+2)	1.57(-5)	1.97(+2)	1.57(-5)
31×31	3.14(+2)	6.97(-6)	3.10(+2)	6.90(-6)	3.21(+2)	6.67(-6)
37×37	4.48(+2)	3.44(-6)	4.46(+2)	3.43(-6)	4.46(+2)	3.43(-6)
43×43	6.09(+2)	1.94(-6)	6.08(+2)	1.93(-6)	6.08(+2)	1.93(-6)
49×49	8.77(+2)	1.18(-6)	7.94(+2)	1.14(-6)	7.94(+2)	1.14(-6)
55×55	1.00(+3)	7.48(-7)	1.00(+3)	7.43(-7)	1.06(+3)	7.42(-7)
61×61	1.32(+3)	5.07(-7)	1.24(+3)	4.91(-7)	1.24(+3)	4.91(-7)
	$O(N^{1.04})$	$O(h^{3.75})$	$O(N^{1.06})$	$O(h^{3.73})$	$O(N^{1.07})$	$O(h^{3.73})$

(a) Uniform grid

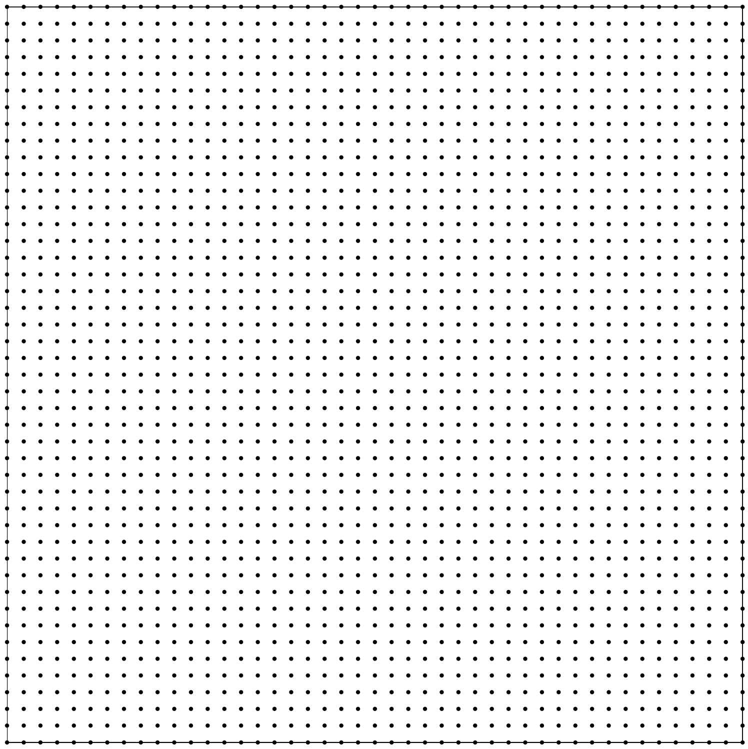

(b) Non-uniform grid

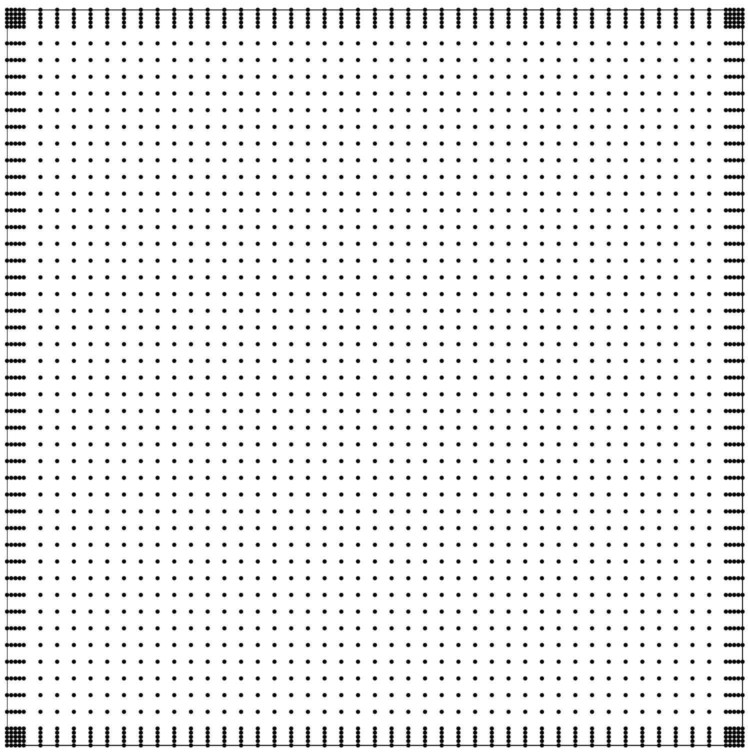

Figure 1: Rectangular domain, point-collocation approach: spatial discretisations.

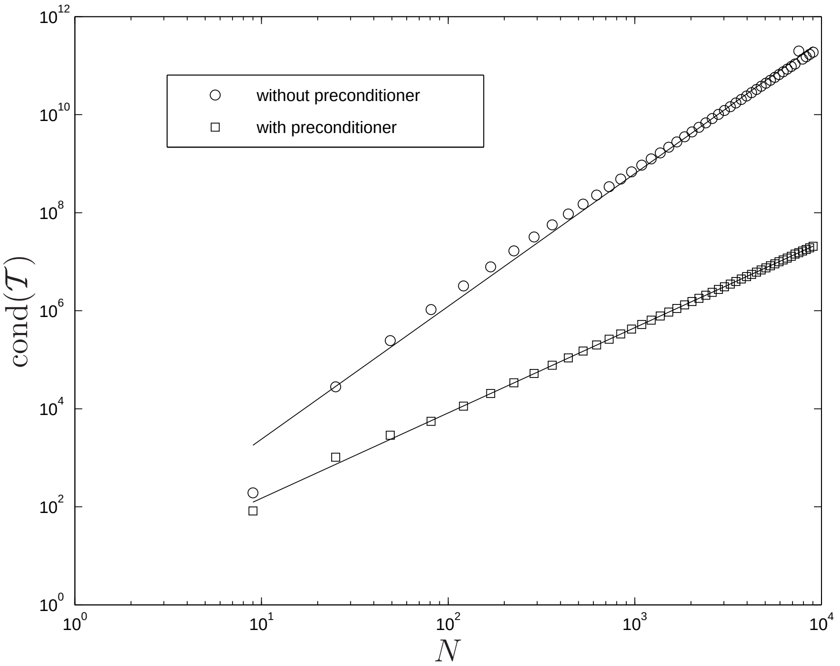

Figure 2: Rectangular domain, point-collocation approach: Condition numbers of the transformation matrix versus the total number of nodal points. The values of N employed are $[9, 25, 49, \cdots, 9025]$.

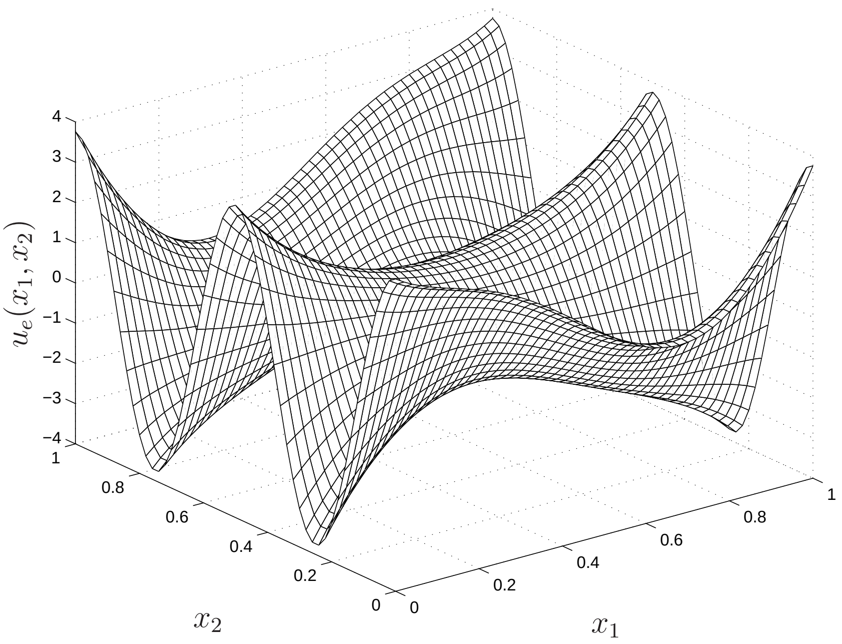

Figure 3: Function $u_e(x_1, x_2) = \sin(\pi(2x_1-1))\sinh(2x_2-1)+\cosh(2(2x_1-1))\cos(2\pi(2x_2-1))$.

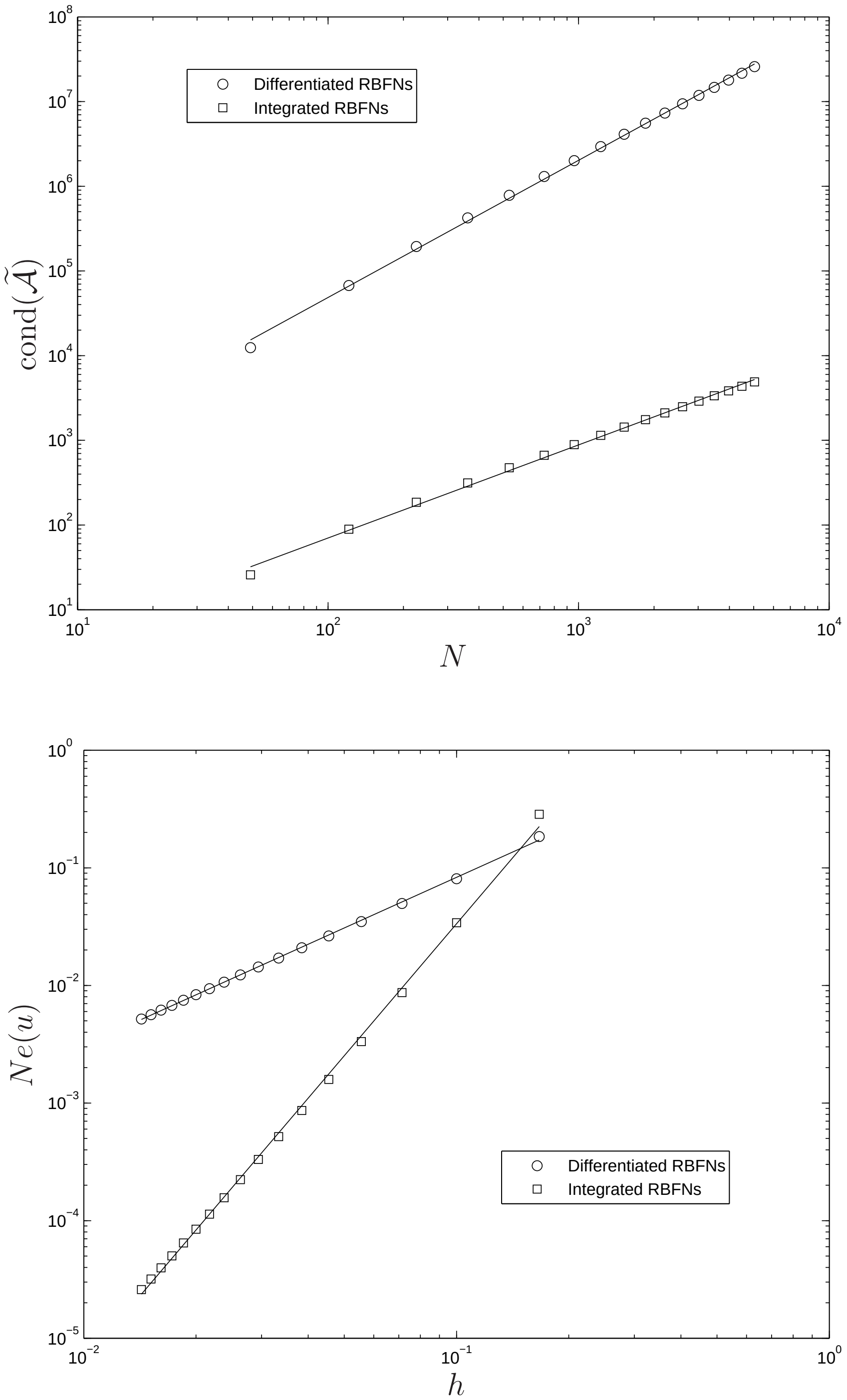

Figure 4: Rectangular domain, point-collocation approach: Condition numbers of the system matrix and errors of the solution by IRBFNs and DRBFNs. The values of N employed are $[49, 121, \cdots, 5041]$.

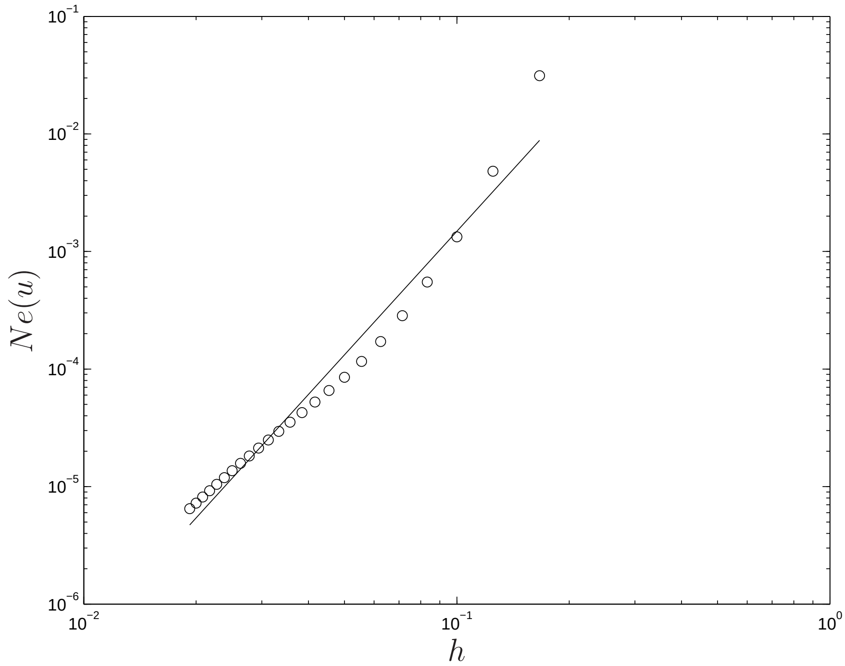

Figure 5: Rectangular domain, point-collocation approach, nonuniform grid: Errors of the IRBFN solution. The values of N employed are $[169, 225, \cdots, 3481]$.

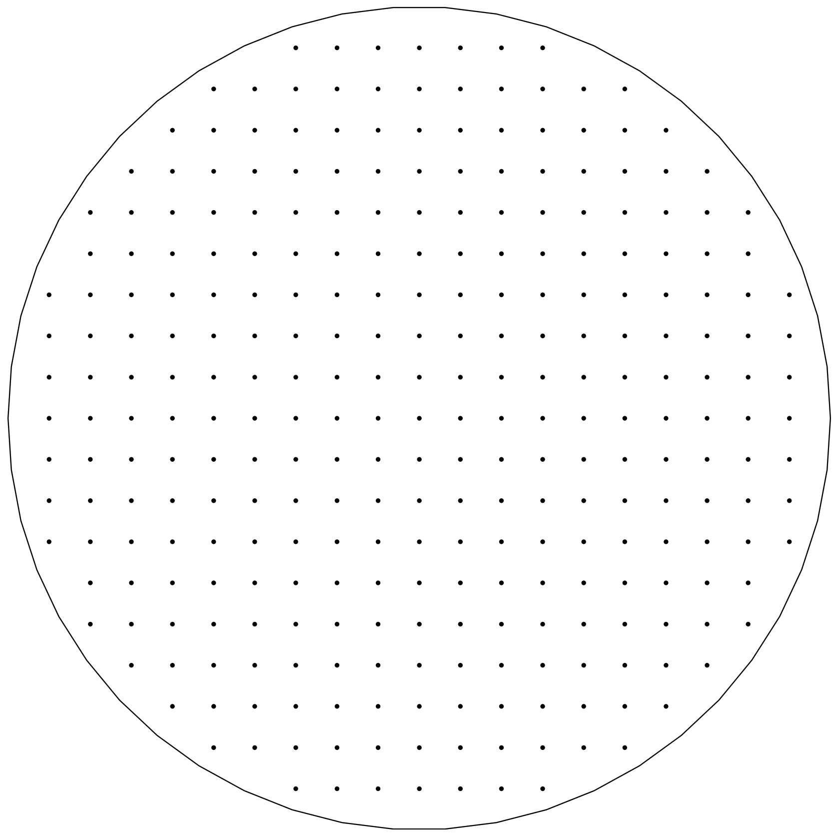

Figure 6: Non-rectangular domain, point-collocation approach, $\Delta = h/4$: spatial discretisation.

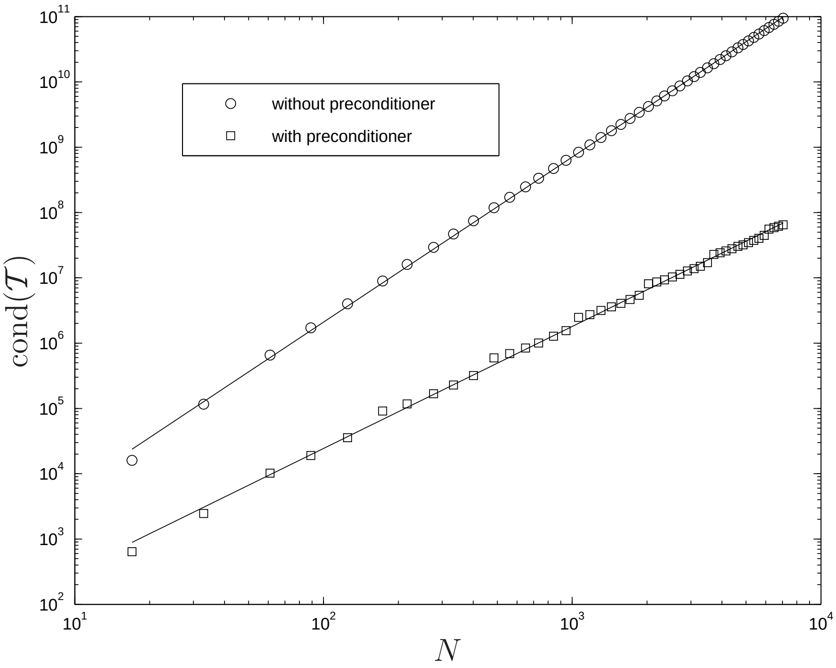

Figure 7: Non-rectangular domain, $\Delta = h/4$: Condition numbers of the transformation matrix versus the total number of nodal points. Grids employed are $[5\times 5, 7\times 7, \cdots, 95\times 95]$.

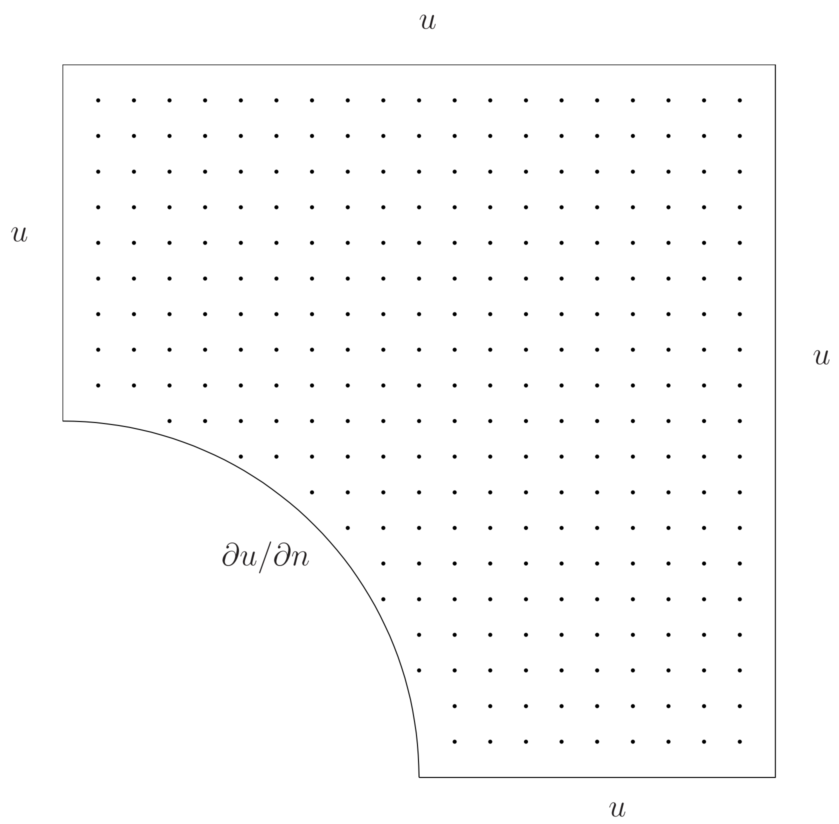

Figure 8: Non-rectangular domain, point-collocation approach, Neumann boundary condition, $\Delta = h/4$: spatial discretisation.

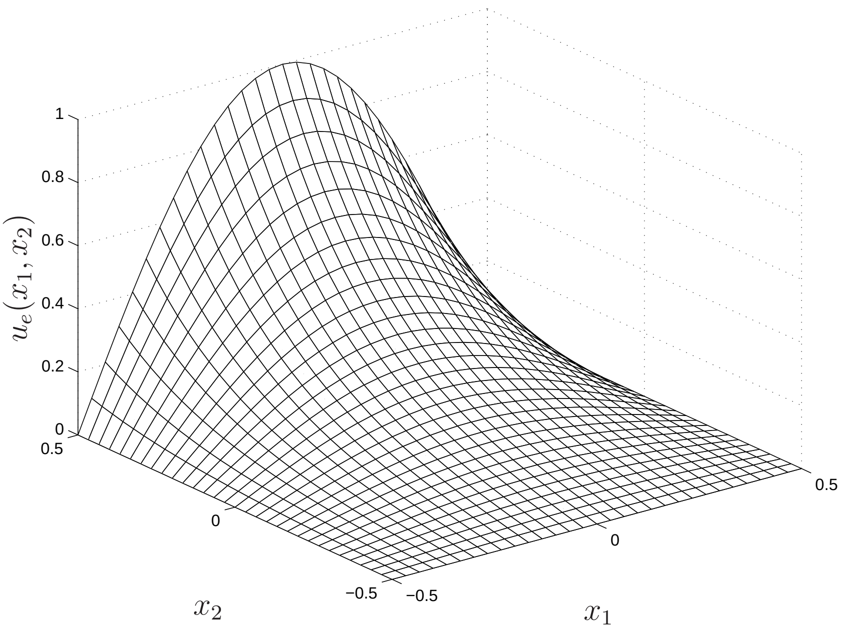

Figure 9: Function $u_e(x_1, x_2) = \frac{1}{\sinh(\pi)} \sin\left(\pi x_1 + \frac{\pi}{2}\right) \sinh\left(\pi x_2 + \frac{\pi}{2}\right)$.

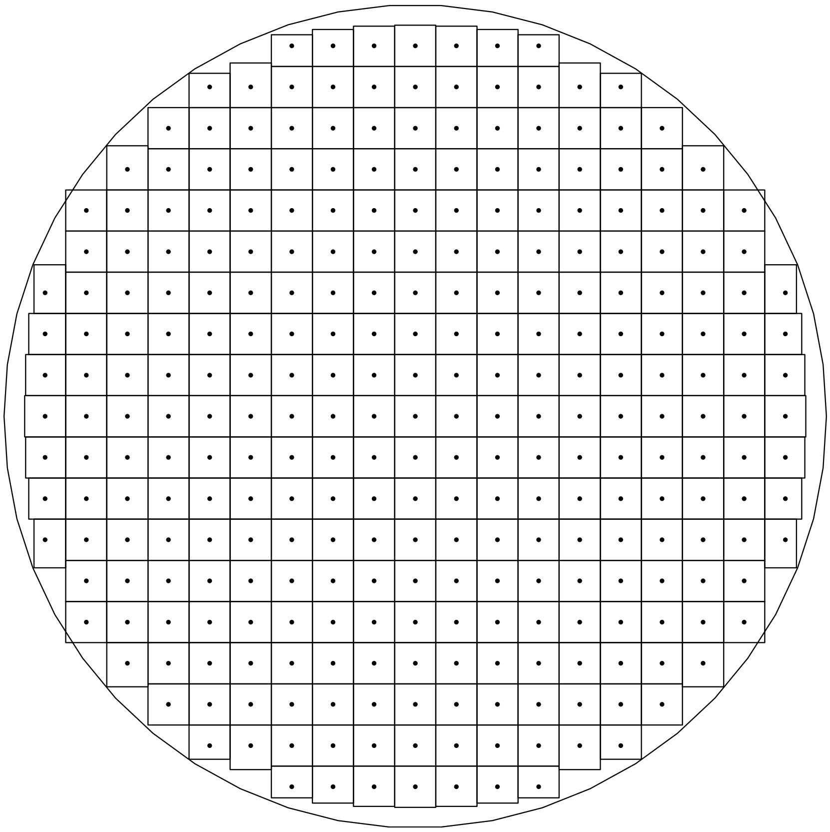

Figure 10: Non-rectangular domain, control-volume approach, $\Delta = h/4$: spatial discretisation.

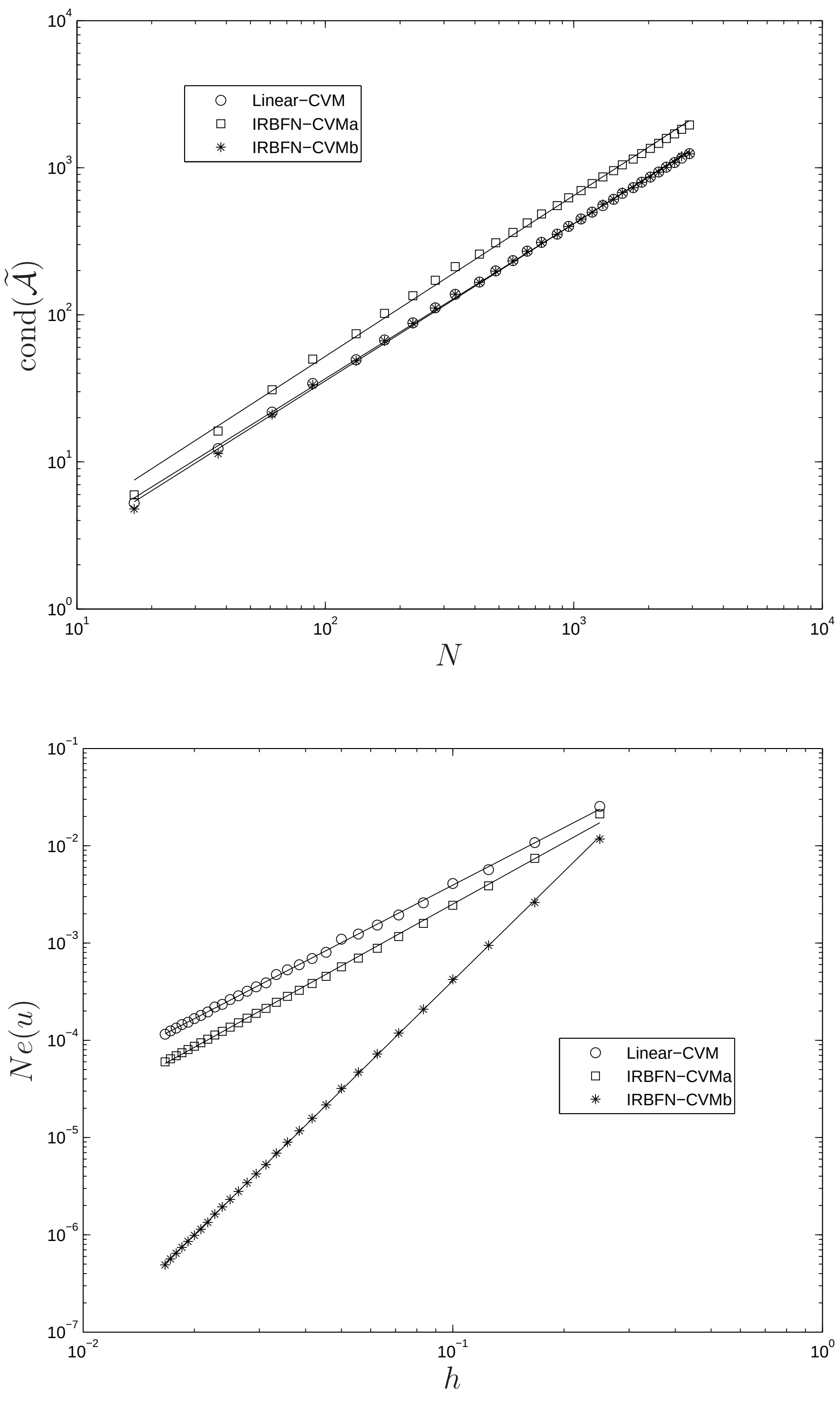

Figure 11: Non-rectangular domain, $\Delta = h/6$, control-volume approach: Condition numbers for the system matrix and errors of the solution by linear-CVM, IRBFN-CVMa (midpoint rule) and IRBFN-CVMb (Gaussian quadrature). Grids used are $[5 \times 5, 7 \times 7, \cdots, 61 \times 61]$.

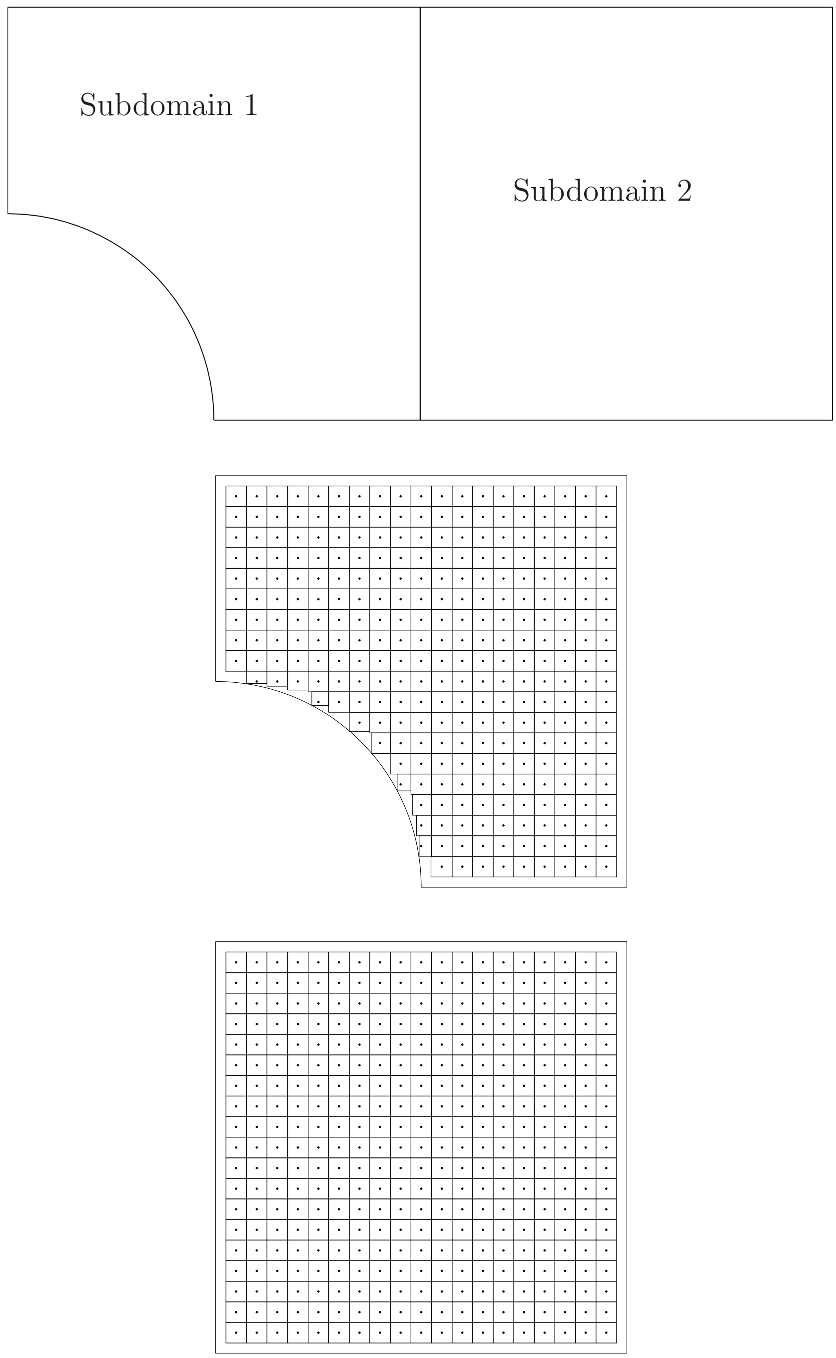

Figure 12: Domain decomposition.

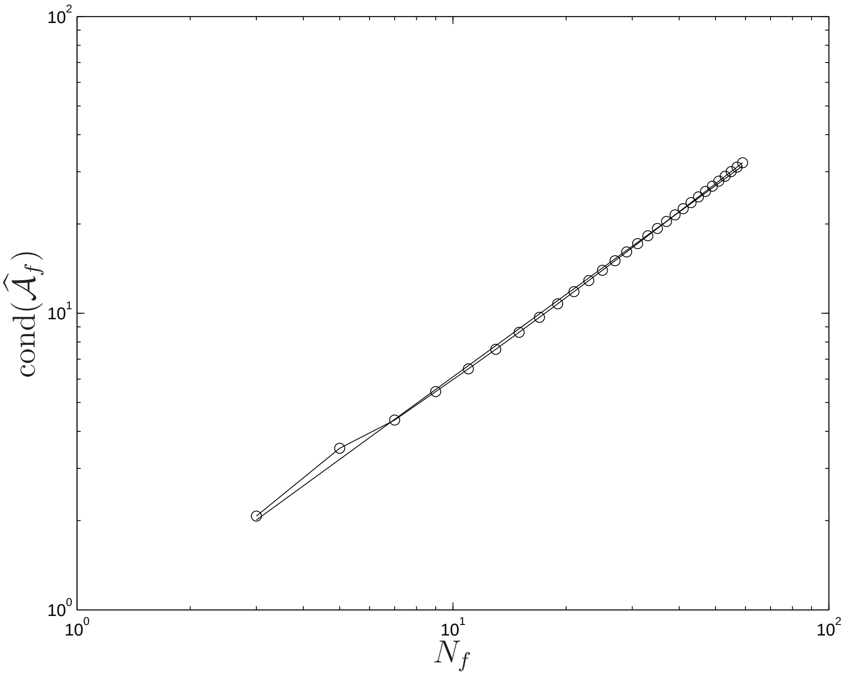

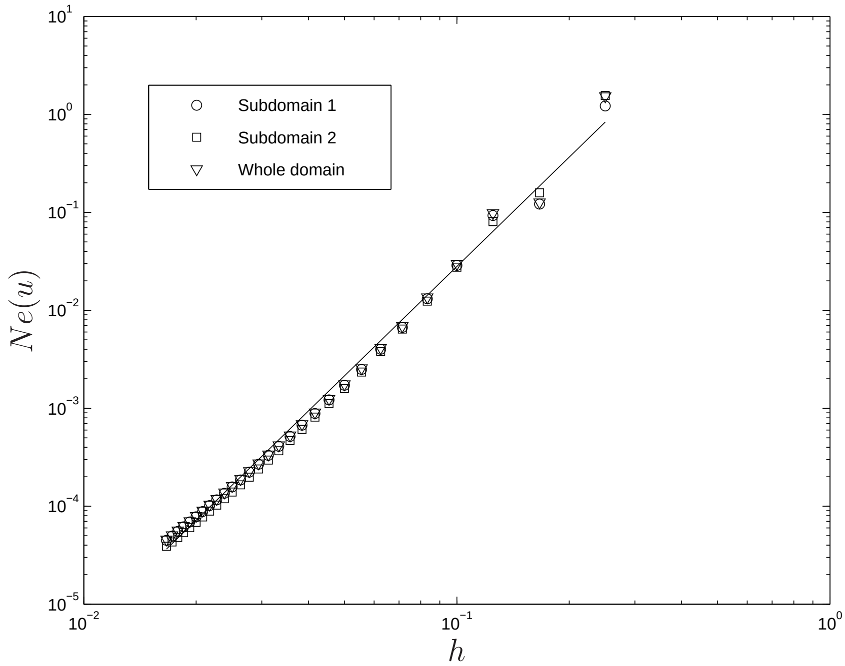

Figure 13: Domain decomposition, control-volume approach: Condition numbers for the interface matrix $\widehat{\mathcal{A}}_f$ and errors for Subdomain 1, Subdomain 2 and the original domain. For each subdomain, grids used are $[5 \times 5, 7 \times 7, \cdots, 61 \times 61]$.